

Application of an Energy-Dependent Instrument Response Function to the Analysis of Neutron Time-of-Flight Data from Cryogenic DT Experiments

Z. L. Mohamed, O. M. Mannion, J. P. Knauer, C. J. Forrest, V. Yu. Glebov, and C. Stoeckl

Laboratory for Laser Energetics, University of Rochester

Neutron time-of-flight (nTOF) detectors are used to diagnose the conditions present in inertial confinement fusion (ICF) and basic laboratory physics experiments performed on an ICF platform. As detailed in Ref. 1, the instrument response function (IRF) of these detectors is constructed by the convolution of two components: an x-ray IRF and a neutron interaction response. The shape of the neutron interaction response varies with incident neutron energy, changing the shape of the total IRF. Analyses of nTOF data that span a broad range of energies must account for this energy dependence in order to accurately infer plasma parameters and nuclear properties in ICF experiments. This method is applied to synthetic data resembling symmetric cryogenic DT implosions to examine the effect of the energy-dependent IRF on the inferred areal density. Results of forward fits that infer ion temperatures and areal densities from nTOF data collected during cryogenic DT experiments on OMEGA are also discussed.

Areal density is a quantity that is used to diagnose the compressive performance of cryogenic DT ICF experiments. With the recent development of a second xylene nTOF line of sight (LOS) on OMEGA that uses the same detector design as an existing OMEGA nTOF,²⁻⁴ an additional measurement of backscatter areal density is now available, enabling the study of implosion symmetry via variations in nTOF areal density.

Analysis of the nTOF data is conducted via forward fit. The standard forward-fit model⁵ can be written as

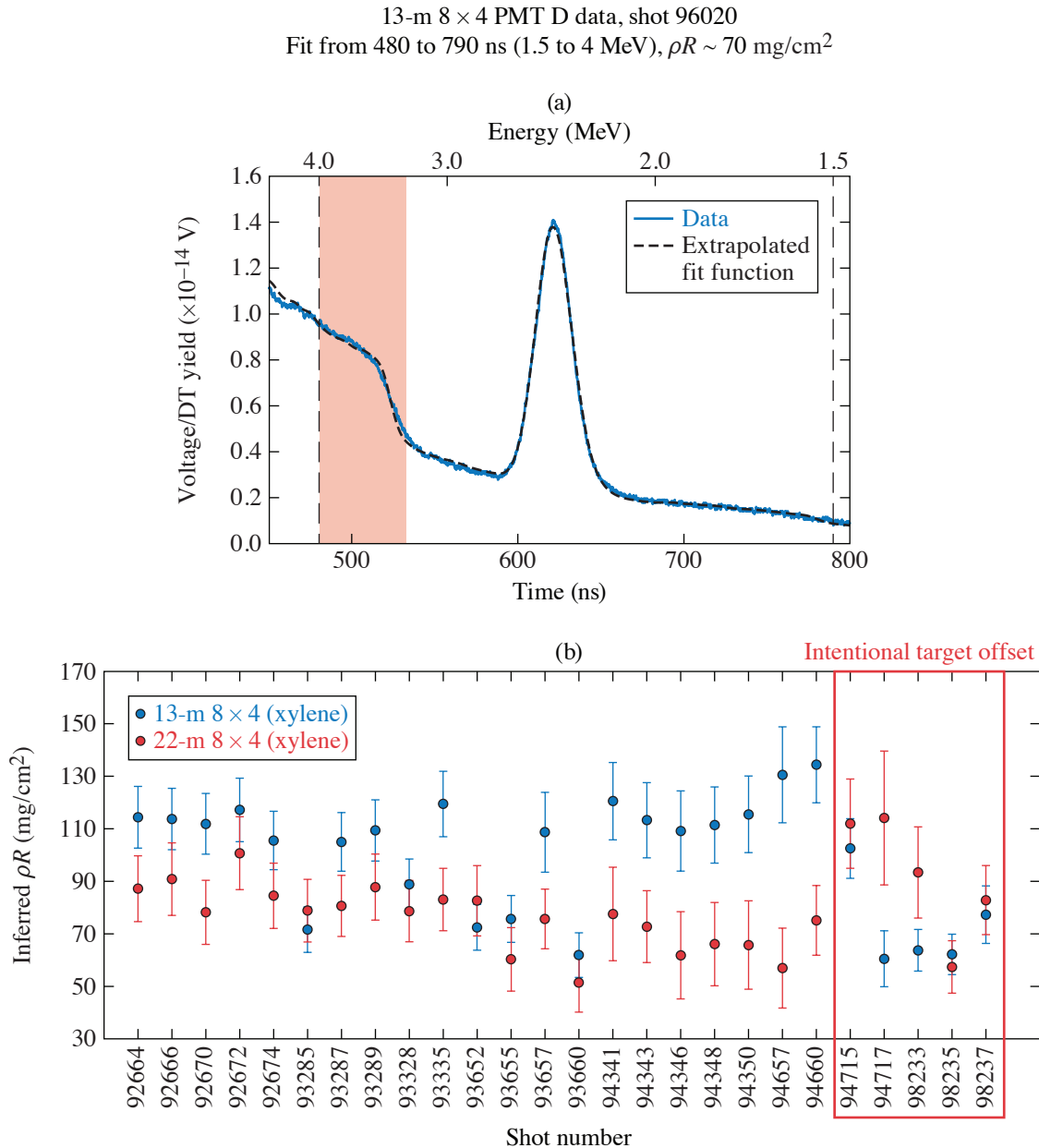
$$V(t) = \left\{ 50 \Omega \times k \times s(E) \times a(E) \times \frac{dN}{dE_{4\pi}} \frac{dE}{dt} \right\} \otimes \text{IRF}(E, t) + B(t), \quad (1)$$

where $V(t)$ represents the fit to the nTOF data in units of volts, k represents a charge calibration constant in units of nC/neutron, 50Ω represents digitizer impedance, $s(E)$ represents detector sensitivity as calculated by MCNP⁶ (a Monte Carlo code) simulations of the xylene detector, $a(E)$ represents beamline attenuation of neutrons as calculated using MCNP simulations of the detector and the LOS from the center of the OMEGA target chamber,⁴ $dN/dE_{4\pi}$ represents the total neutron spectrum exiting the ICF target into 4π , dE/dt represents the relativistic Jacobian, IRF represents the total instrument response function, \otimes represents convolution, and B is a background model. For these detectors, the background is represented by an exponential decay function and is mainly associated with the scattering of DT neutrons on structures near the detector's LOS. For cryogenic DT implosions, the energy spectrum $dN/dE_{4\pi}$ contains contributions from the DD primary, TT, and n(D,p)2n reactions as well as the neutrons that scatter elastically on D and T within either the hot spot or the cold fuel shell (i.e., nD and nT elastic single scatters). Since areal densities on OMEGA are relatively low ($<350 \text{ mg/cm}^2$), a spectrum for multiple scatters is not currently included in this model.

The model spectra for nD and nT elastic single scatters are built such that

$$\frac{dN}{dE_{nT+nD}} = \rho L \times Y_{DT} \times \frac{\int_{3.3 \text{ MeV}}^{4 \text{ MeV}} \left[f_T \frac{d\sigma_{nT}}{dE} + f_D \frac{d\sigma_{nD}}{dE} \right] dE}{f_T m_T + f_D m_D}. \quad (2)$$

Note that the use of this equation assumes a point source of neutrons and uses the elastic scattering cross sections for DT neutrons on D and T. The model for the $n(D,p)2n$ spectrum comes from the cross sections inferred in Ref. 7. This spectrum also scales with areal density and is calculated similarly to Eq. (2), but using the $n(D,2n)p$ cross section in Ref. 7. In this model, it is assumed that the nT and nD elastic single scatters and the $n(D,2n)p$ components represent the same areal density. An example of the total fit is shown in Fig. 1.



E29437JR

Figure 1

(a) Example of a forward fit to experimental nTOF data for the 13-m xylene detector. The blue curve represents the data while the black curve represents the fit. The vertical dashed lines indicate the range of the fit (1.5 to 4 MeV). The red shaded area represents the region in which nT and nD single-scatter components of the fit are integrated to calculate a backscatter areal density (3.5 to 4 MeV). (b) Areal densities for several shots as inferred by the forward fit outlined in this work. The 22-m LOS generally infers about 20 mg/cm² lower than the 13-m LOS. With imposed target offsets based on the measured flow velocities, the direction of the asymmetry can be reversed or the asymmetry can be minimized.

Recent developments in the analysis of nTOF data at the Omega Laser Facility include the analysis of a larger range of energies (1.5 to 4 MeV). Analysis over this wide range of energies allows one to more accurately determine the background, which affects the inferred spectra of nD and nT single elastic scatters. Because this analysis spans a wide range of energies, it is most accurate to use an energy-dependent IRF as detailed in Ref. 1. The final fit has six parameters. Four parameters are related to the neutron energy spectrum: DD ion temperature, DD mean energy, DD yield, and areal density. The background is modeled as an exponential decay. The remaining two parameters in the forward fit are the magnitude and time decay constant for the background. The final inferred areal density is calculated by inverting Eq. (2), where the integrated energy spectra are the best-fit spectra for the elastically scattered nD and nT neutrons. Note that this analysis focuses on the backscattered nT neutrons by integrating over 3.3 to 4 MeV.

This analysis has been benchmarked using synthetic data that represent symmetric, isobaric implosions. The neutron energy spectra were generated using an ice block model in *IRIS3D*.⁸ Synthetic nTOF data were then generated using Eq. (1) along with these energy spectra. The data set involved here represents isobaric 2-keV implosions with areal densities from 50 to 250 mg/cm². The forward fits to the synthetic data were carried out using the method that was previously detailed, which is also applied to experimental data.

The forward-fit analysis with an energy-dependent IRF recovers the ρL calculated directly from the *IRIS3D* energy spectra almost exactly. If either the 2.45-MeV or 3.5-MeV monoenergetic IRF is used, ~2%–3% inaccuracy is introduced. This is a relatively small inaccuracy with the current analysis, which spans 1.5 to 4 MeV, because the only sharp features within this region are the DD signal (2.45 MeV) and the nT edge (3.5 MeV), which are relatively close in energy. For these detectors, the difference in the width of the IRF's is relatively small between 2.45 and 3.5 MeV (~0.7-ns difference in FWHM). The inaccuracy introduced with the use of a monoenergetic IRF is expected to grow substantially if the range of the fit is extended to 9 MeV, although the exact magnitude of the effect has not yet been predicted because a more-advanced energy spectrum model and a different method of determining the background will likely be required to reach this goal.

The forward fit described above is designed to be applicable for approximately symmetric implosions; however, asymmetric implosions can be more complicated. Since the n(D,p)2n spectrum is known to be forward-peaked while this analysis focuses on the elastically backscattered nD and nT neutrons, these spectra may not scale by the same areal densities as this analysis assumes. It is assumed that the differences between the realistic asymmetric spectrum and the modeled symmetric spectrum will go into the “background” component of the fit. It is for this reason that the background is not fixed. Changes in the background (i.e., background from environmental scattering + any asymmetric contributions) have been observed in experimental data.

The current analysis using the fit for background parameters along with the symmetric nD and nT elastic scatter and n(D,2n)p models has been applied to cryogenic data dating back to early 2019 (when the second nTOF LOS came online on OMEGA). With the standard beam-pointing procedure and no imposed target offset, the 22-m LOS, which views part of the lower hemisphere of the target, sees an average of 20 mg/cm² lower areal densities than the 13-m LOS, which views part of the upper hemisphere of the target. Variations in these inferred nTOF areal densities are consistent with measured variations in ion temperature.⁹ As shown in Fig. 1, this trend has been reversed with intentionally imposed target offsets based on measured flow velocities. In other instances, strategic target offsets based on flow velocity^{9,10} have been used to minimize the areal-density asymmetry. The ability to minimize or reverse the direction of the areal-density asymmetry indicates that the areal-density measurement responds as expected when a mode-one perturbation is minimized or reversed in direction. These instances of minimized differences in areal densities along the two LOS correspond to shots with minimal ion temperature asymmetries as well as flow velocities.¹⁰

Future work will include further benchmarking of this analysis with asymmetric synthetic data. This will test the current handling of the background as well as the scaling of the different components [i.e., nT elastic scatters versus nD elastic scatters versus n(D,2n)p, which originate from different parts of the shell] and should additionally reveal any sensitivities of the current analysis to the exact shape of the nT, nD, and n(D,2n)p spectra under asymmetric conditions.

This material is based upon work supported by the Department of Energy National Nuclear Security Administration under Award Number DE-NA0003856, the University of Rochester, and the New York State Energy Research and Development Authority.

1. Z. L. Mohamed *et al.*, J. Appl. Phys. **128**, 214501 (2020).
2. C. Stoeckl *et al.*, Rev. Sci. Instrum. **81**, 10D302 (2010).
3. V. Yu. Glebov *et al.*, Rev. Sci. Instrum. **85**, 11E102 (2014).
4. C. J. Forrest *et al.*, Nucl. Instrum. Methods Phys. Res. A **888**, 169 (2018).
5. R. Hatarik *et al.*, J. Appl. Phys. **118**, 184502 (2015).
6. X-5 Monte Carlo Team, Los Alamos National Laboratory, Los Alamos, NM, Report LA-UR-03-1987 (2008).
7. C. J. Forrest *et al.*, Phys. Rev. C **100**, 034001 (2019).
8. F. Weilacher, P. B. Radha, and C. Forrest, Phys. Plasmas **25**, 042704 (2018).
9. O. M. Mannion *et al.*, Rev. Sci. Instrum. **92**, 033529 (2021).
10. O. M. Mannion *et al.*, Nucl. Instrum. Methods Phys. Res. A **964**, 163774 (2020).